Polythiolactone-Decorated Silica Particles: A Versatile Approach for Surface Functionalization, Catalysis and Encapsulation

Dustin Werner Kurka+,[a] Maximilian Niehues+,[a] Sergej Kudruk,[b] Volker Gerke,[b] and Bart Jan Ravoo*[a]

Abstract: The surface chemistry of colloidal silica has tremendous effects on its properties and applications. Commonly the design of silica particles is based on their de novo synthesis followed by surface functionalization leading to tailormade properties for a specific purpose. Here, the design of robust "precursor" polymer-decorated silica nano- and microparticles is demonstrated, which allows for easy post-modification by polymer embedded thiolactone chemistry. To obtain this organic-inorganic hybrid material, silica particles (SiO$_2$P) were functionalized via surface-initiated atom transfer radical polymerization (SI-ATRP) with poly(2-hydroxyethyl acrylate) (PHEA)-poly(thiolactone acrylamide (PThlAm) co-polymer brushes. Exploiting the versatility of thiolactone post-modification, a system was developed that could be used in three exemplary applications: 1) the straightforward molecular post-functionalization to tune the surface polarity, and therefore the dispersibility in various solvents; 2) the immobilization of metal nanoparticles into the polymer brushes via the in situ formation of free thiols that preserved catalytic activity in a model reaction; 3) the formation of redox-responsive, permeable polymer capsules by crosslinking the thiolactone moieties with cystamine dihydrochloride (CDH) followed by dissolution of the silica core.

Introduction

Colloidal silica is of immense interdisciplinary interest in many fields of applications such as coatings, chromatography, biotechnology and pharmaceutics. The vast number of advantageous properties, e.g. controllable size and shape, large surface area, outstanding physical and chemical stability, biocompatibility and well established surface chemistry, turns it into an ubiquitous material.[1,2] Especially the surface chemistry is a dominant factor, as it allows to finely tune the surface properties of particles and therefore the interaction with their environment.[3–5] In this way it is possible to endow the surface of colloidal silica with new functionalities, thus expanding the applicability into new fields like drug delivery,[1,6] imaging agents,[1,7,8,9] catalytic supports,[1,10] biosensors,[11] templates for polymer capsules[12,13] or self-assembly.[14–16] The functionalization of silica particles is usually achieved by two main strategies. On the one hand the one-pot synthesis via the co-condensation of different silica or alcohol sources.[4,17] On the other hand there is the post-functionalization using grafting methods.[3,5,9,18] Independent of which method is favored in detail, the modified particles are usually designed to fulfil a specific purpose for a certain application. To be used in other applications, it is therefore often necessary to adjust the synthetic parameters according to the new requirements. Hence, developing a toolbox particle system that allows for simple modification with several functional groups under mild conditions would be highly desirable. Recently, such an example was reported by Cattoën and Wong Chi Man.[19] They presented a general method to prepare multi-functional mesoporous silica nanoparticles with homogeneously distributed functionalities. By co-condensation of clickable azide and alkyne organosilanes with a silica source they were able to combine the advantageous features of both approaches. The homogeneous distribution of functionalities as well as the post-functionalization by copper-catalyzed cycloaddition (CuAAC) enables the divergent synthesis of particles and molecular precursors from well documented synthetic protocols. However, the copper catalyst necessary for the CuAAC limits biological applications. Another very interesting class of compounds for versatile post-functionalizations under mild conditions are thiolactones that can

[a] D. W. Kurka,+ M. Niehues,+ Prof. Dr. B. J. Ravoo
    Organic Chemistry Institute/Center for Soft Nanoscience
    Westfälische Wilhelms-Universität Münster
    Corrensstraße 36, 48149 Münster
    and
    Busso-Peus-Straße 10, 48149 Münster (Germany)
    E-mail: b.j.ravoo@uni-muenster.de

[b] S. Kudruk, Prof. Dr. V. Gerke
    Institute of Medical Biochemistry, Center for Molecular Biology of Inflammation
    Westfälische Wilhelms-Universität Münster
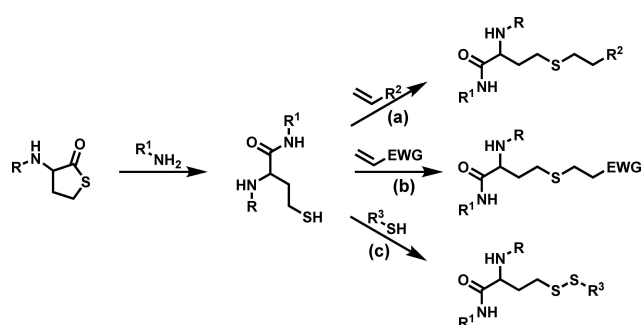   Von-Esmarch-Straße 56, 48149 Münster (Germany)

[+] These authors contributed equally to this work.

undergo an aminolysis step and subsequently react with thiols, alkenes or Michael acceptors in a one-pot synthesis (Scheme 1).[20]

In numerous examples, Du Prez and co-workers demonstrated the ease of functionalization for this class of molecules by designing oligomers and polymers either with thiolactones as monomeric unit[21] or as post-modifiable group.[22] Moreover, due to the ability to convey multifunctionality, thiolactones are used for growing dendrimers,[23] forming emulsions[24] and gels[25] and modifying solid supports like gold[26] or silicon[27] surfaces. Although, thiolactones feature a large variety of possibilities in terms of post-functionalization only very few reports address surface modifications of particles with thiolactones.[28] Herein, we present a toolbox approach utilizing polymer decorated silica particles as a precursor that can easily

introduce multiple functionalities for a wide range of different applications. Our system is based on colloidal silica modified with statistical co-polymer brushes incorporated with thiolactone moieties (PSiO$_2$NP). The co-polymer brushes equip the particles with important surface properties, specifically: a high density of homogeneously distributed functional groups as well as a high colloidal stability by steric repulsion. In addition, the thiolactones enable derivatization under very mild conditions (ambient atmosphere, no catalyst etc.) with a large variety of functionalities by using amines and thiols or Michael acceptors. Structurally inherent, the two appended molecules are in close proximity that could potentially be used for interaction or synergetic effects between them, such as energy transfer or dual catalysis. In this work, we further demonstrate the versatility and applicability of our system as a template for various heterogenous catalysis by the immobilization of metal nanoparticle into the polymer, as a template to form permeable polymer capsules potentially capable of drug delivery and on-demand release and as a way to allow the simple functionalization of our particles with different molecules that can feature e.g. light responsiveness or define the polarity of the particles (Scheme 2).

Scheme 1. Schematic overview of thiolactone-based synthetic approaches for post-modification. The aminolysis of a thiolactone is followed either by a thiol-ene conjugation via (a) a radical (UV-initiated) or (b) a nucleophilic (thiol-Michael) addition or by (c) a disulfide formation.[20]

Results and Discussion

Preparation of precursor particles (PSiO$_2$NP)

SiO$_2$NP with an average size of 67 nm were obtained following a modified Stöber method.[29] According to previous works of
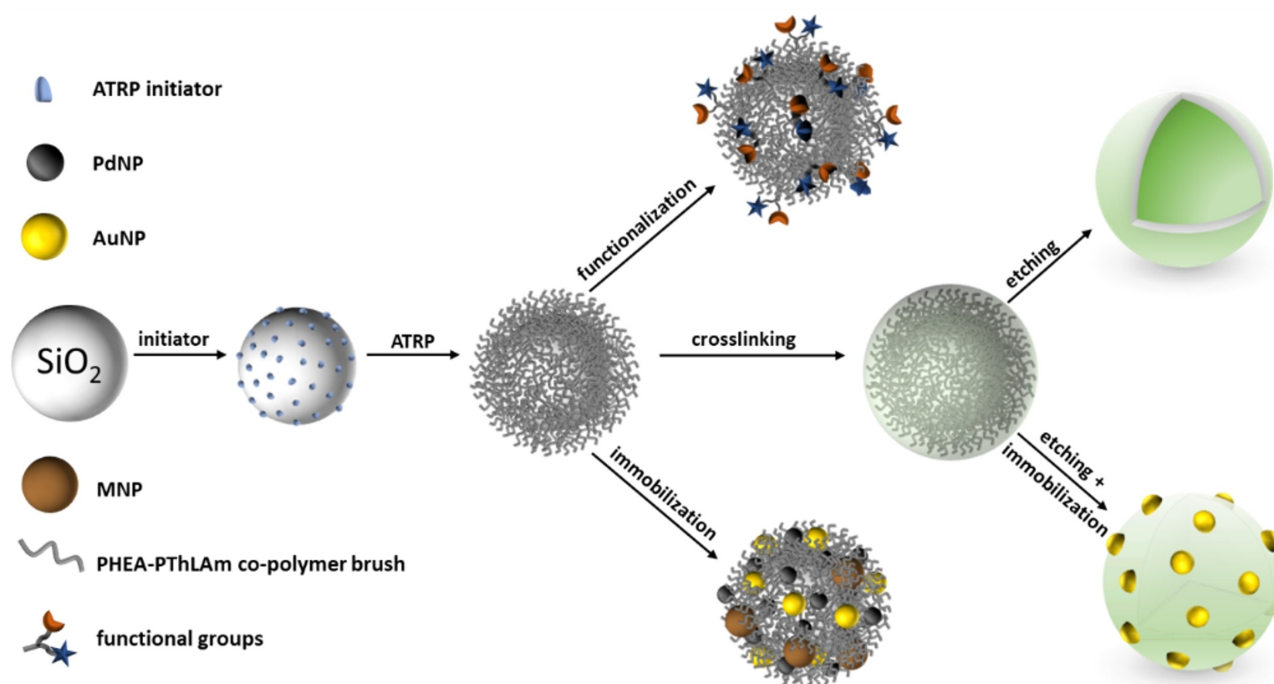

Scheme 2. Synthesis of precursor silica particles functionalized with PHEA-PThLAm co-polymer brushes and their post-modification by molecular functionalization, immobilization of metal nanoparticles, or crosslinking and capsule formation.

Chemistry–A European Journal

Full Paper
doi.org/10.1002/chem.202100547

Chemistry Europe
European Chemical
Societies Publishing

our group,[14,15] we functionalized the SiO_2NP with polymer brushes in order to generate a high density of functional groups as well as to gain a high colloidal stability due to steric repulsion. Therefore, the particles were pre-functionalized with an ATRP initiator followed by the co-polymerization of HEA and ThLAm yielding our PHEA-PThLAm co-polymer functionalized precursor particles ($PSiO_2NP$) (Scheme 3). Detailed information about the particle preparation is provided in the Supporting Information.

Dynamic light scattering (DLS) and transmission electron microscopy (TEM) revealed the size of the SiO_2NP before (Figure S1a) and after the surface-initiated polymerization. Compared to the bare NP, an increase of 128 nm in hydrodynamic diameter (d_H) can be detected for the PHEA-PThLAm functionalized NP (Figure 1a). This indicates the successful functionalization of the silica cores with a roughly 64 nm thick polymer shell. We observed that d_H remains constant upon washing with various solvents and sonication, indicating stable anchoring of the polymer to the particle surface. Considering that the d_H provides an overestimation of the thickness due to solvation of the polymer brushes, we also investigated the thickness of the polymer brushes in TEM. Here we found the distinct formation of a polymer shell of about 15 nm in the dried state (Figure 1b and Figure S1b). It is known that in the dried state the polymer brushes collapse and form a dense shell around the NP core which leads to a size underestimation via TEM. GPC measurements of the residual polymer after dissolution of the silica core resulted an average molecular weight (M_n) of 1.13×10^6 g/mol.

To further determine the polymer content on the NP surface, we measured the weight loss by thermogravimetric analysis (TGA). Figure 1c shows the TGA curve for the $PSiO_2NP$

up to 1000 °C. An immense weight loss of around 74% between 200 °C and 500 °C followed by reaching a plateau was observed for the polymer decorated NP. This indicates that a large amount of organic material covers the silica cores. The slight decrease in weight at low temperature (< 200 °C) is due to the evaporation of water physically adsorbed on the particle surface. The contribution to weight losses caused by the continued condensation reaction of silanol groups and associated water loss between 200 °C and 500 °C should have a neglectable impact in our case (around 6% for bare silica), as roughly 75% of our polymer decorated NP consists of organic material.[30] Combining the GPC and TGA results, we calculated the grafting density of the polymer brushes and determined a density of 0.037 chains/nm².[31] We note that although the grafting density of the polymer is rather low, their average molecular weight is very high, resulting in a dense surface coating of the particles with polymer brushes. The polymer composition (molar ratio of HEA and ThLAm) on the particles was estimated by ¹H-NMR. Therefore, a polymer sample was formed in solution from free initiator and purified (Figure S2). The measured ratio of co-monomers (15 mol% ThLAm) was similar to the monomer feed in the polymerization. Moreover, IR spectra of the $PSiO_2NP$ showed the characteristic ester carbonyl group ($\nu_{C=O} = 1730$ cm^{-1}) and C–H stretching vibration ($\nu_{CH} = 2850$–2980 cm^{-1}) of the acrylic polymer backbone (Figure S3).[32] These results support the successful modification of the particles with the desired polymer.
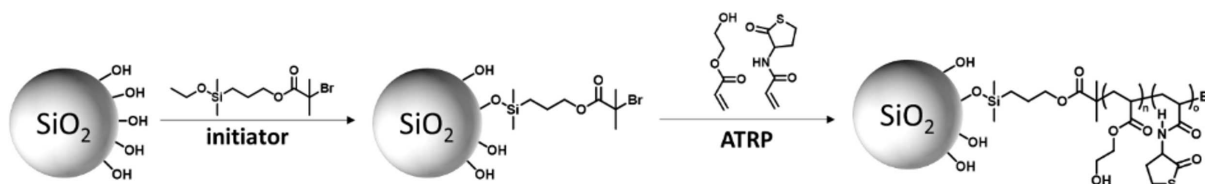
Scheme 3. Pre-functionalization of silica particles with the ATRP initiator followed by the co-polymerization of HEA and ThLAm.

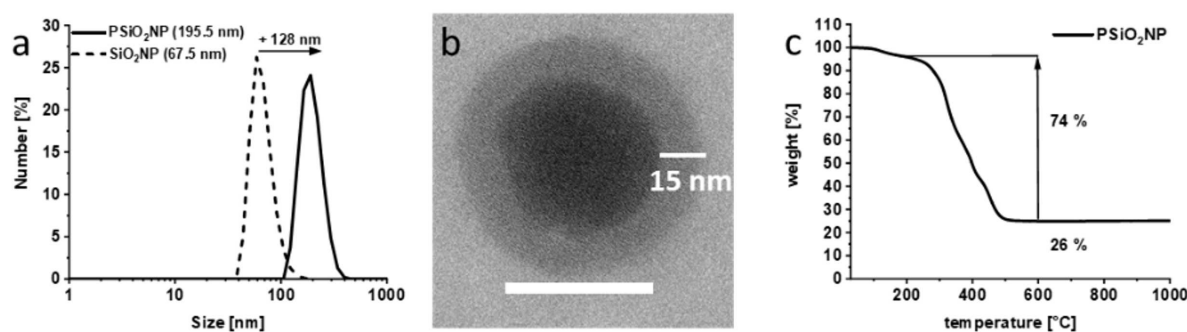**Figure 1.** Determination of size (DLS, TEM) and polymer content (TGA) of the hybrid $PSiO_2NP$. (a) Hydrodynamic radius (d_H) of SiO_2NP in DMF before and after functionalization with PHEA-PThLAm polymer brushes. (b) TEM image of an unstained $PSiO_2NP$ particle showing the silica core and the polymer shell. Scale bar: 50 nm. (c) TGA graph indicating the weight loss depending on temperature for the $PSiO_2NP$.

Chemistry–A European Journal

Full Paper
doi.org/10.1002/chem.202100547

**Chemistry
Europe**
European Chemical
Societies Publishing

Molecular post-modification

Our initial goal was to demonstrate the ease of post-modification for the precursor particles by addressing both crucial functionalities in our system. Therefore, we used the arylazopyrazole (AAP) photoswitch,[33] which allows for an easy UV/vis detection to verify the successful post-functionalization. One the one hand, we used an AAP–NH$_2$ to test the aminolysis reaction of the thiolactone. On the other hand, a mixture of ethanolamine and an AAP–SH was chosen to verify one-pot aminolysis followed by a disulfide bond formation. With the help of tris(2-carboxyethyl)phosphine (TCEP) as mild reducing agent, we could further show the redox-responsive behavior of the disulfide by releasing the AAP-SH again from the particles. In both cases, the particle dispersed in DMF were simply mixed with the reactants and stirred at room temperature overnight. The purified particles were then dissolved in DMF and characterized by UV/vis spectroscopy. In contrast to the unfunctionalized particles, the UV/vis spectrum of AAP–NH$_2$ functionalized particles clearly displays the typical AAP absorbance with its striking π-π^* transition band at 338 nm and the n-π^* absorbance at 423 nm (Figure S4a). Similar observations were made for the AAP–SH modified particles, confirming the successful functionalization by the aminolysis reaction and the subsequent formation of disulfides (Figure 2a). We also measured the supernatant solution after the last purification step to confirm that the absorbance was not caused by remaining AAP in solution (Figure 2a). For investigating the redox responsiveness, we exposed the AAP–S–S–PSiO$_2$NP to a reductive environment using TCEP. Both, the purified particles and the supernatant solution were investigated after the reduction using UV/vis spectroscopy (Figure 2c). Hardly any absorbance of the AAP is left in the particle dispersion whereas the supernatant displays high absorbance of the corresponding AAP–SH.

In addition, irradiation experiments with UV light (365 nm) and green light (520 nm) revealed the well-preserved reversible photoswitchability of the *E* to *Z* isomerization for both AAP–NH$_2$ and AAP–SH immobilized on the particle surface (Figure 2b and Figure S4b). For at least five cycles the AAPs were perfectly switchable without any loss in absorbance intensity at 338 nm. Furthermore, we attempted to estimate the lowest number of thiolactone moieties accessible for the AAP–NH$_2$ in the polymer

brushes. Therefore, we calibrated the AAP-NH$_2$ between 1 μM and 100 μM and calculated the amount of AAP on the particles to be approximately 0.13 μmol/mg (Figure S4c,d), which is equivalent to the lowest number of thiolactone moieties accessible. In addition, based on the results of the TGA analysis and ^{1}H-NMR measurement we roughly calculated the amount of ThLAm theoretically incorporated in the polymer. Assuming that around 74% of the material is polymer with 15% thiolactone content, the maximum particle concentration of ThLAm is 0.89 μmol/mg. We believe, the discrepancy between these two values can be explained by incomplete yields presumably caused by the limited accessibility of the thiolactone moieties in the interior of the polymer brush shell. These results were considered later for the crosslinking experiments prior to the formation of polymer capsules.

To further demonstrate the possibilities for post-modifications of our precursor particles, we utilized molecules of different polarity to affect the dispersibility in different solvents. Hexadecylamine (HDA) and the polyamine spermine were exemplarily used for the functionalization of PSiO$_2$NP with nonpolar or polar molecules, respectively. The simple addition of each amine to the particles dispersed in DMF resulted in the formation of HDA-PSiO$_2$NP and spermine-PSiO$_2$NP functionalized particles, which were confirmed by IR spectroscopy (Figure S5). An increase of the C–H stretching vibration ($\nu_{CH} = 2850$–2980 cm^{-1}) compared to the PSiO$_2$NP is indicating the presence of (CH$_2$) groups in the HDA molecule (Figure S5a). Furthermore, the resulting particles were not dispersible in polar solvents such as water anymore, which is a strong indicator for the reduced surface polarity. The spermine functionalized particles exhibited an increase of the absorption band at around 3300 cm^{-1} which can be attributed to the $\nu_{NH2, NH}$ stretching modes. The appearance of the bands between 1320–1650 cm^{-1} can be attributed to $\nu_{NH2, CH2}$ scissor and ν_{NH} bend bands,[34] both indicating the presence of spermine (Figure S5b). In addition to the changes in the IR spectrum, we could also measure an increase of the zeta potential from $\zeta = -33$ mV for the PSiO2NP to $\zeta = +24$ mV for the spermine-PSiO$_2$NP. Furthermore, these particles were only dispersible in water and aggregated in organic media, both again validating the change in surface polarity of the polymer.

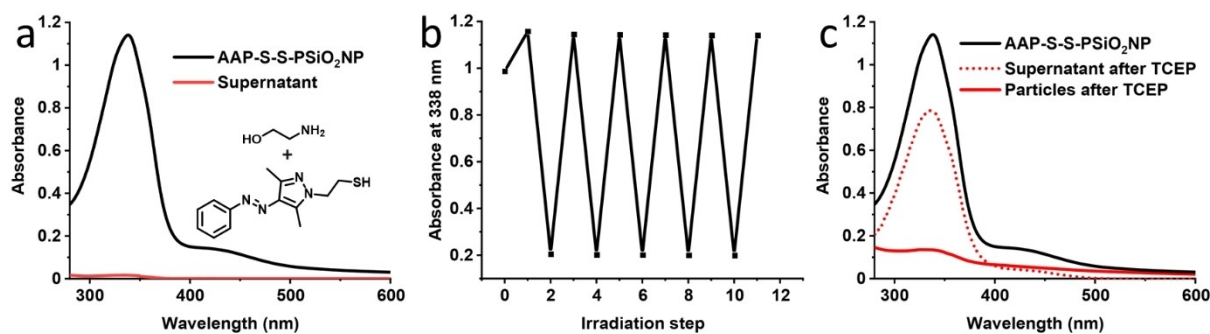**Figure 2.** UV/vis spectra of the AAP–S–S–PSiO$_2$NP (a) and the photoisomerization of the immobilized AAP–SH in DMF (b). Irradiation times: 10 s (365 nm) and 30 s (520 nm). (c) UV/vis spectra of the same particles after incubation with TCEP in DMF.

Chemistry–A European Journal

Full Paper
doi.org/10.1002/chem.202100547

Chemistry
Europe
European Chemical
Societies Publishing

Immobilization of metal nanoparticles

Our precursor particles at hand, we wanted to further illustrate the versatility of our post-modifiable particles by immobilizing metal NP into the polymer brushes. Attaching metal NP to a support material can feature synergistic properties and can be important to improve their colloidal stability, handling and their utility i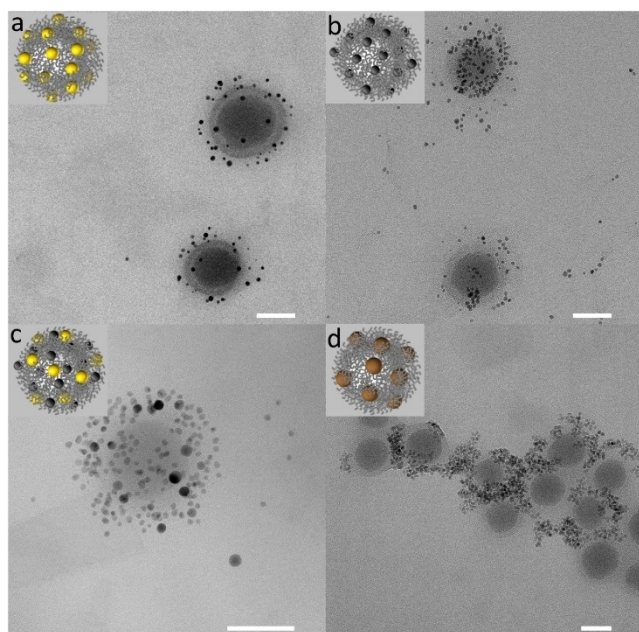n a range of applications.[4,7,35] In addition, clusters or controlled assemblies of metallic and inorganic NP are able to enhance the relevant physical properties and cooperative functions as compared to the individual particles.[36] Here, we used dodecylamine (DDA) stabilized gold NP (AuNP), oleylamine (OlAm) stabilized palladium NP (PdNP) and 3-aminopropyltriethoxysilan (APTES) functionalized magnetic $CoFe_2O_4$ NP (MNP) for the immobilization experiments. Au and Pd can endow the precursor particles with catalytic or imaging functionalities, whereas the MNP can implement magnetic properties e.g. for magnetic separation. Initially, we simply mixed AuNP (Figure 3a), PdNP (Figure 3b), a mixture of both (Figure 3c) or MNP (Figure 3d) together with our $PSiO_2NP$ to form the NP assemblies (detailed experimental procedures can be found in the Supporting Information). TEM measurements revealed the successful immobilization of the precursor particles with each type of metal NP (Figure 3 and S6) and showed significantly less free NP not located on the precursor support.

Figure 3. Representative TEM images of immobilized AuNP (a), PdNP (b), AuNP/PdNP (c) and MNP (d) on $PSiO_2NP$. Scale bars: 50 nm.
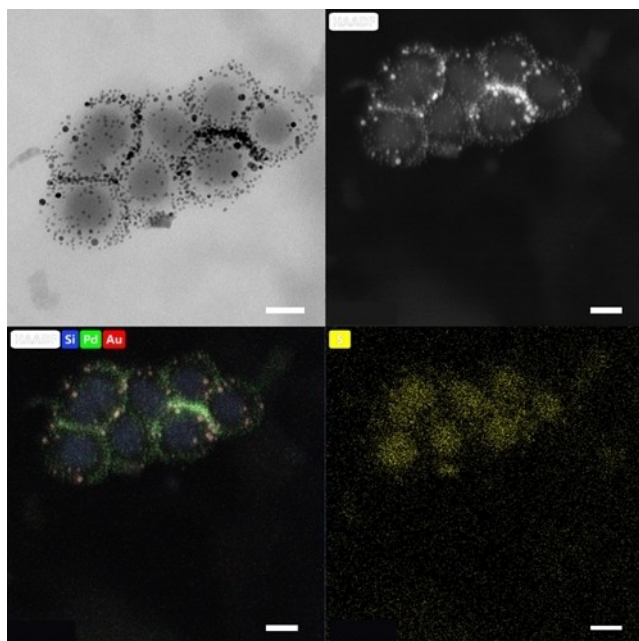
Additionally, a HAADF-EDX mapping for the sample with mixed AuNP and PdNP immobilized on the $PSiO_2NP$ displays the localization of the elemental distribution of the system. The mapping confirms the presence of AuNP and PdNP covering the silica core as well as the presence of sulfur from the ThLAm in the polymer (Figure 4 and Figure S7). We propose that for Au and Pd the NP are immobilized due to the aminolysis reaction of the amine ligands with the thiolactone and the subsequent *in situ* formation of free thiols. These thiols are known to be strongly binding and well stabilizing ligands for noble metal NP. In the case of APTES functionalized MNP the free amine can directly form a covalent bond to the thiolactone moieties within the polymer brushes leading to the NP immobilization. As shown in Figure 3d, the MNP are, in contrast to the individually distributed AuNP and PdNP, clustered. This is possibly caused by a partial aggregation during the ligand exchange with APTES. However, the images show that the MNP clusters are located solely on the polymer, indicating that the immobilization mechanism is driven by the aminolysis reaction. In these proof of principle experiments we demonstrated the versatility of our precursor particles for the immobilization of various NP utilizing thiolactone chemistry.

Focusing on the prominent class of Au–SiO_2 hybrid materials,[37] we proceeded to optimize the immobilization of AuNP and to apply the assemblies in the catalytic reduction of 4-nitrophenol as a model reaction. Moreover, we found supporting evidence for our assumption that the immobilization is driven by the attractive interaction between the AuNP and the *in situ* formed free thiols. We assume that the number of AuNP immobilized on the $PSiO_2NP$ is in proportion to the number of free accessible thiols. Therefore, our goal was to maximize the aminolysis of the thiolactone prior to the NP immobilization by adding an excess of ethylene diamine (EDA) to the $PSiO_2NP$ dispersion. Thus, the affinity of the polymer brushes towards the NP should be increased in a twofold manner. On the one hand we maximized the number of accessible thiols as the strong binding ligand for noble metal NP. On the other hand, we introduced additional amine groups increasing the local concentration of binding moieties and therefore enhancing the multivalent driving force for the

Figure 4. BF-TEM image and HAADF-EDX mapping of mixed AuNP and PdNP immobilized on $PSiO_2NP$. Scale bars: 50 nm.

Chemistry–A European Journal

Full Paper
doi.org/10.1002/chem.202100547

Chemistry Europe
European Chemical
Societies Publishing

immobilization of the NP. Both are contributing to the stabilization of AuNP which we observed in a higher number of NP localized on the polymer-decorated particle surface (Figure 5a and Figure S8a,b). Furthermore, UV/vis spectroscopy of the NP assemblies identified the typical distinct surface plasmon resonance (SPR) band of AuNP at 532 nm indicating the immobilization of individual stabilized AuNP rather than aggregated species for which a higher SPR band wavelength would be expected (Figure 5b). Notably, control experiments using simply PHEA functionalized SiO_2NP (PHEA–SiO_2NP) without thiolactone moieties under otherwise similar conditions did not show the typical SPR band for AuNP (Figure S9a). In contrast to our precursor particles, the PHEA–SiO_2NP are not able to stabilize the AuNP in the form of red colored assemblies but rather lead to AuNP aggregation accompanied by the characteristic purple color (Figure S9b,c).

The catalytic activity of the gold-supported catalyst AuNP–$PSiO_2NP$ was investigated for the well-known reduction of 4-nitrophenol at room temperature in the presence of $NaBH_4$. The catalytic reaction was monitored by UV/vis spectroscopy as described in the Supporting Information. The time dependent degradation of 4-nitrophenol catalyzed by the gold-supported catalyst is presented in Figure 5c. Upon addition of the catalyst, the absorbance at $\lambda = 400$ nm, which is characteristic for nitrophenolate ions in basic media, decreased and a new absorbance band at $\lambda = 300$ nm arose corresponding to the formation of 4-aminophenol. To evaluate the activity and recyclability of the catalyst, the particles were separated from the reaction medium by centrifugation and reused after washing in four further cycles. For each cycle a substrate conversion of over 99% was reached indicating a high catalytic activity and reusability of the AuNP–$PSiO_2NP$ catalyst (Figure 5c and Figure S8c,d).

Formation of redox responsive polymer capsules

Further, we utilized our precursor particles as a scaffold to form redox responsive polymer capsules permeable for mass transfer and redox-degradable in the presence of TCEP under mild conditions. Hollow containers are of great interest due to their unique properties and promising application in different fields like material science, catalysis or biomedicine.[38] Especially the application as drug delivery vehicles makes polymer capsules particularly attractive as they can accommodate high payloads with improved efficiency, reduced toxicity and side effects, and can be modified for targeting and controlled release of the therapeutic agents.[12,39] Herein, we used nano- and micron-sized precursor particles for the formation of polymer capsules. By simply crosslinking the thiolactone moieties within the polymer brushes using the diamines EDA or CDH (Scheme S1) followed by the etching of the templating silica core with a buffered oxide etch (BOE), we obtained non-degradable (for EDA) or redox-responsive (for CDH) polymer capsules. DLS measurements as well as TEM and SEM images showed that the capsules with mean diameters of $d_H = 175$ nm and $d_H = 1.1$ μm for the PnCapsules and PμCapsules, respectively, maintained approximately the same size as before etching (Figure 6a and Figure S1c,d). Interestingly, in the dried state (for TEM and SEM), the polymer nano-capsules appeared as spheres (Figure 6b and Figure S10a) whereas the micro-capsules are rather plum-like shaped (Figure 6c, d and Figure S10b,c). The latter appearance is most likely due to the larger size and the hollow interior causing the soft polymer shell to collapse under solvent free conditions. Removal of solvent and collapse also explains the change in size for the PμCapsules in one dimension (Figure S1d).

To obtain redox-responsive polymer capsules, we used cystamine as disulfide bridging crosslinker. Exposed to a reductive environment or a competitive thiol, like the biorelevant glutathione, the disulfide bonds are cleaved due to reduction or to disulfide exchange reaction, which leads to a disassembly of the capsules. Starting from the micron sized capsules the addition of TCEP as reducing agent resulted in the successful degradation of capsules and the formation of undefined polymer structures (<150 nm) (Figure 6e,f and Figure S11a–c). In order to take up or release molecules the polymer shell has to be permeable to allow the mass transfer. Therefore, to demonstrate the potential applicability of the polymer capsules for drug delivery, we performed confocal laser scanning microscopy (CLSM) to visualize the uptake of rhodamine b as model compound (Figure 7). Utilizing the *in situ* formed free thiol during the crosslinking process, we introduced NBD-SH as a second functionality to obtain fluorescently-labeled capsules (Figure S12).

For the time-dependent analysis of the rhodamine b uptake, the NBD-labeled capsules were first diluted in water, transferred to an ibidi slide and placed on ice for one hour in order to
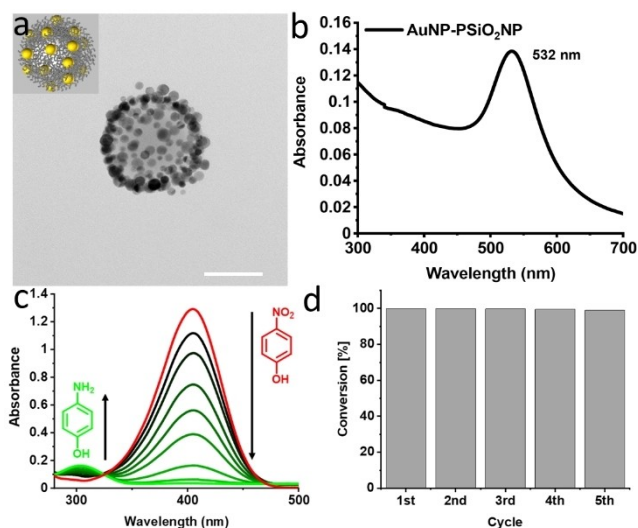

Figure 5. Characterization of the AuNP–$PSiO_2NP$ assemblies formed under optimized conditions and their use in a catalytic model reaction. (a) TEM image of AuNP immobilized on $PSiO_2NP$. Scale bar: 50 nm. (b) UV/vis spectra of the AuNP-$PSiO_2NP$ assemblies in DMF. (c) UV/vis absorbance spectra showing the reduction of 4-nitrophenol to 4-aminophenol using the AuNP-$PSiO_2NP$ assemblies as catalyst. (d) Calculated conversion of 4-nitrophenol for five consecutive reduction cycles based on the monitored UV/vis spectra.
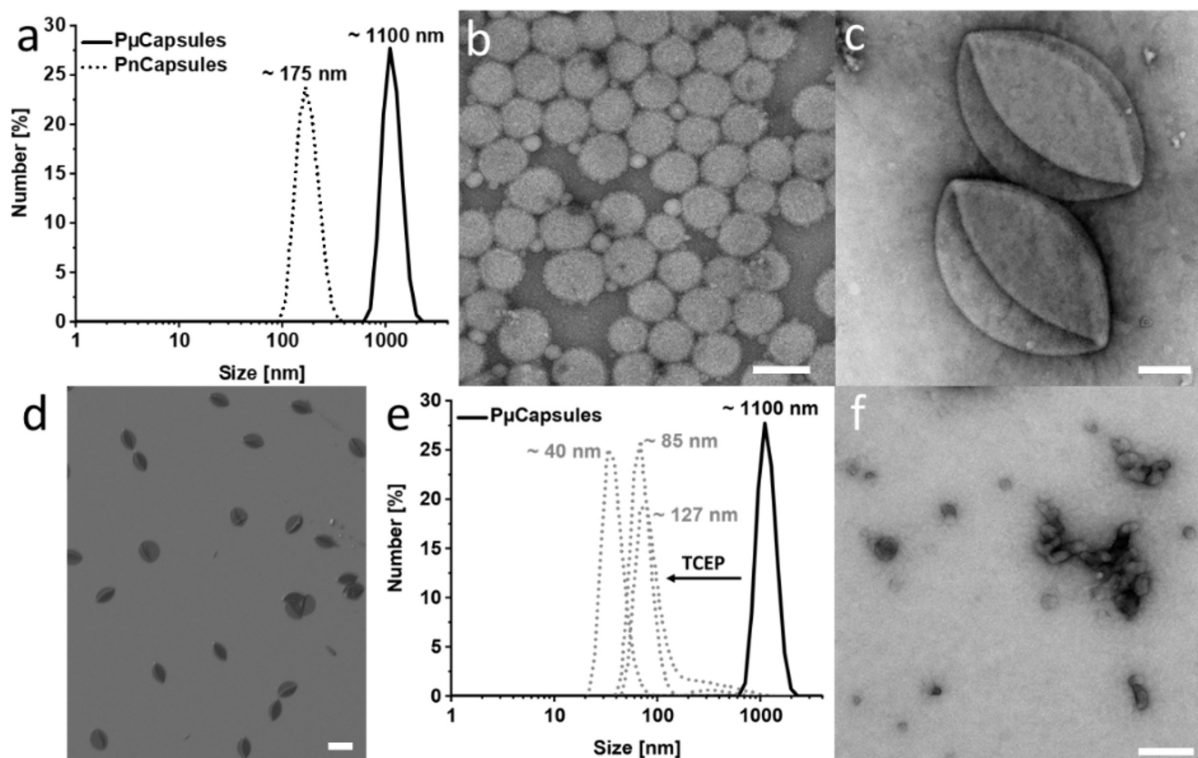
Chemistry–A European Journal

Full Paper
doi.org/10.1002/chem.202100547

Chemistry Europe
European Chemical
Societies Publishing

Figure 6. (a) Size distribution of nano- (PnCapsules) and micro-capsules (PµCapsules) in DMF. (b) TEM image of EDA crosslinked PnCapsules. Scale bar: 200 nm. (c) TEM image of CDH crosslinked plum-shaped PµCapsules. Scale bar: 500 nm. (d) SEM image of CDH crosslinked PµCapsules. Scale bar: 2 µm. (e) DLS graph of CDH crosslinked PµCapsules before and after degradation with TCEP in DMF. (f) TEM image of the degraded PµCapsules. Scale bar: 200 nm. TEM samples were negatively stained before measurement.
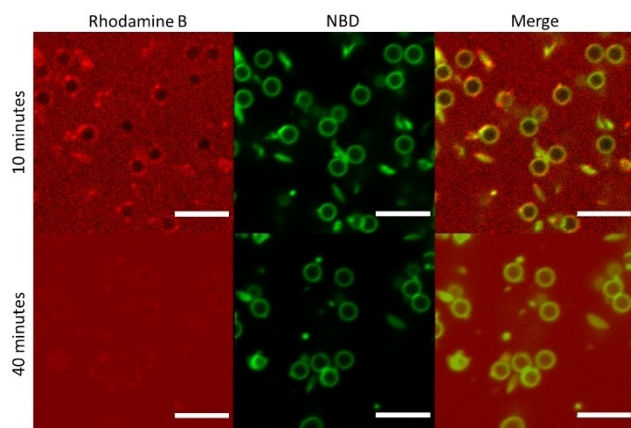

Figure 7. CLSM images of rhodamine b uptake into the NBD-labeled PµCapsules. Images were taken after 10 min (top) and approximately 40 min (bottom). Scale bars: 5 µm.

decrease their mobility. Then, rhodamine b was added and CLSM was performed to follow the dye uptake. Images were taken after incubation at room temperature for 10 min, 20 min (not shown here), 40 min and 90 min (not shown here), respectively. Initially, the interior of the polymer capsules appeared as dark spot presenting the absence of rhodamine b at the beginning of incubation (Figure 7, top). Over time the dye is able to diffuse into the capsules as indicated by the red

fluorescence distributing within the capsules. In less than 40 min, complete diffusion of the model compound can be observed (Figure 7, bottom), demonstrating the permeability of the polymer capsules and the potential use for triggered delivery of payload.

Combining both approaches, the immobilization of metal nanoparticles and the formation of capsules, we were also able to obtain polymer capsules decorated with AuNP. This kind of system might be interesting as dual treatment for e.g. cancer therapy by combining photothermal ablation therapy (PTA) and drug delivery as well as potential photoacoustic imaging. PTA is a therapeutic strategy in which irradiated near infrared light (NIR) is converted into heat to damage and destroy cancer cells.[40] Therefore, the SPR band of gold nanoparticles has to be tuned from the visible region to NIR to reach the "therapeutic window" of 700 nm to 1400 nm. An example for shifting the SPR band of AuNP towards longer wavelength was demonstrated previously via ripening of AuNP on cyclodextrin vesicles.[41] Aside from that, this could also be addressed by the immobilization of anisotropic gold nanorods with their characteristic NIR absorbance.

Here, we first crosslinked the polymer shell of the precursor particles (PSiO$_2$NP and PSiO$_2$µP) with CDH under oxygen free conditions to prevent the oxidation of *in situ* formed thiols. In a next step, we simply mixed these crosslinked particles together with AuNP to immobilize the NP on our precursor. The

Chemistry–A European Journal

Full Paper
doi.org/10.1002/chem.202100547

Chemistry Europe
European Chemical
Societies Publishing

dissolution of the silica template as a final step yielded our polymer capsules decorated with AuNP (Figure 8 and Figure S13). UV/vis measurements (Figure 8a,d) as well as TEM images (Figure 8b,c and e and Figure S1e) confirmed a dense coverage of the capsule surface with AuNP, which are, however, still individually stabilized indicated by the distinct SPR band of around 530 nm.

Conclusion

The preparation of co-polymer decorated silica particles is a facile approach for diverse post-modifications. By exploiting the beneficial properties of thiolactones for the straightforward post-modification with different functionalities, we created precursor particles easily adjustable towards various applications. Thus, we were able to demonstrate the post-functionalization of silica particles with fluorophores and photoswitches, the immobilization of various metal nanoparticles and their use in the catalytic reduction of 4-nitrophenol, as well as the formation of redox responsive, permeable polymer capsules decorated with AuNP. We anticipate that our concept can serve as variable toolbox for many more applications, since the straightforward post-modification with amines, thiols, alkynes or Michael acceptors establishes a wide variety of possibilities.

Experimental Section

Preparation of ATRP initiator functionalized SiO_2NP

3-Dimethylethoxysilylpropyl-2-bromoisobutyrate (10 vol%) as ATRP initiator was added to the SiO_2NP dispersed in DMF (ca. 260 mg in 4 mL DMF) and the mixture was stirred at 80 °C for 15 h. The initiator functionalized particles were purified by centrifugation (11,000 rpm, 20 min) and redispersion in DMF (3×).

Functionalization of SiO_2NP with PHEA-PThLAm co-polymer brushes ($PSiO_2NP$)

HEA (2-hydroxyethyl acrylate) (1.01 g, 8.68 mmol) was mixed with ThLAm (262 mg, 1.53 mmol, 15 mol%) in a *Schlenk* tube under argon atmosphere. Then, ATRP initiator functionalized SiO_2NP (ca. 260 mg) in DMF (1 mL) were added. To this mixture, a solution (1 mL) of $Cu(II)Br_2$ (5 mg, 22 μmol) and Tris-[2-(dimethylamino)ethyl]amine (36 mg, 110 μmol) in DMF (10 mL) and a solution (5 μL) of ethyl α-bromoisobutyrate (62 mg, 0.32 mmol; EBIB) in DMF (0.95 mL) as co-initiator were added. The tube was subjected to four freeze/thaw cycles, and after adding ascorbic acid (20 mg, 0.11 mmol), the reaction mixture was stirred at 85 °C for 48 h. The particles were collected by centrifugation (11,000 rpm, 20 min) and purified by redispersion in DMF (4×) before storing them in a stock solution of 8.62 mg/mL in DMF (20 mL). The polymer grown in solution was dissolved in Milli-Q and precipitated from acetone (3×) in order to remove unreacted monomers. To determine the composition, the pure PHEA-PThLAm co-polymer was characterized by ^1H-NMR.
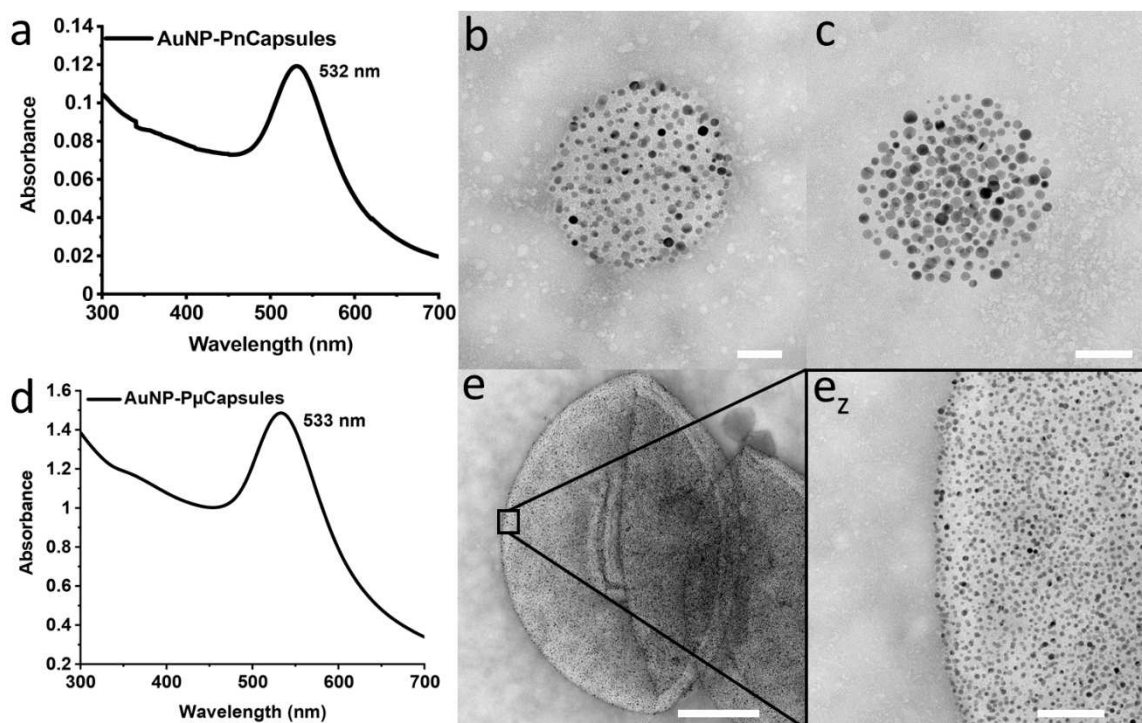

Figure 8. UV/vis spectra and TEM images of AuNP decorated PnCapsules and PμCapsules. (a) UV/vis spectra of AuNP-PnCapsules in DMF. (b,c) TEM images of AuNP-PnCapsules with (b) and without (c) staining of the organic material. Scale bars: 50 nm. (d) UV/vis spectra of AuNP–PμCapsules in DMF. (e) TEM images of stained AuNP–PμCapsules. (e_z) zoom in of (e). Scale bars: 500 nm (e), 100 nm (e_z).

Chemistry–A European Journal

Full Paper
doi.org/10.1002/chem.202100547

Chemistry Europe
European Chemical
Societies Publishing

Preparation and functionalization of silica microparticles (SiO₂μP)

Silica microparticles were obtained from microParticles GmbH as 5% w/v aqueous suspension with average diameters of 0.977 μm (standard deviation (SD) = 0.026 μm). Prior to use, the particles (1.5 mL, 75 mg) were solvent exchanged to DMF by centrifugation (10,000 rpm, 3 min) and redispersion. The functionalization of micro particles with ATRP initiator and PHEA-PThLAm co-polymer brushes (PSiO₂μP) were carried out similar to the procedures of PSiO₂NP. Stock solution: 17.68 mg/mL in DMF (5 mL).

Preparation of polymer capsules

Polymer capsules were obtained by crosslinking the thiolactone moieties within the polymer brushes with either EDA or CDH and the subsequent dissolution of the silica core by etching with buffered oxide etch (BOE 6:1). In detail, 250 μL of polymer functionalized particles (PSiO₂NP or PSiO₂μP) were mixed with 250 μL DMF in a small glass vial. Then, 6×2 μL of either an EDA (30 mM) or a CDH/NEt₃ (30 mM/60 mM) stock solution were added in one-hour intervals before adding 0.2 μL or 0.7 mg of pure EDA or CDH, respectively, as the final step. After stirring overnight, the particles were purified by centrifugation (10,000 rpm, 20 min) and redispersion in DMF and Milli-Q (2×). In order to dissolve the silica core, the particles dispersed in 500 μL Milli-Q were mixed with 1 mL of BOE 6:1 (NH₄F/HF buffer) at room temperature for 4 h. The precipitated hollow polymer capsules were purified by washing with Milli-Q (3×) and finally dispersed in DMF (1 mL) using sonication.

General method for the immobilization of metal nanoparticles on PSiO₂NP

In proof of principle experiments, we immobilized MNP, PdNP and AuNP under not optimized conditions into the polymer brushes of our PSiO₂NP. Therefore, the metal nanoparticles (0.3–0.5 mg) dispersed in toluene (AuNP, PdNP) or EtOH (MNP) were added to a mixture of 50 μL of PSiO₂NP in 0.5 mL toluene/DMF (v/v 1:1). Using an orbital shaker, the particles were allowed to assemble overnight. The nanoparticle assemblies were purified by centrifugation (10,000 rpm, 20 min) and redispersion in toluene/DMF (v/v 1:1) and DMF (2×).

Optimized procedure for the immobilization of AuNP on PSiO₂NP (AuNP-PSiO₂NP)

A dispersion of 50 μL PSiO₂NP in 250 μL DMF was degassed by sonication for one hour. EDA (4.5 mg, 75 μmol) was added under oxygen free conditions and the mixture was stirred overnight. The particles were purified by centrifugation (10,000 rpm, 20 min) and redispersion in DMF (0.5 mL). Half of the particle dispersion was added to a mixture of AuNP (0.4 mg) in toluene (0.5 mL) before placing the vial on an orbital shaker for 18 h. The nanoparticle assemblies were purified by centrifugation (10,000 rpm, 20 min) and redispersion in toluene/DMF (v/v 1:1) and DMF (2×) before storing in a stock solution of DMF (1 mL), which was used for the catalytic reduction of 4-nitrophenol as nanocatalyst.

Preparation of AuNP decorated polymer capsules

Polymer capsules decorated with AuNP were prepared by combining the procedures of "Polymer Capsules" and the "Optimized Procedure for the Immobilization of AuNP-PSiO₂NP". First, a dispersion of 50 μL PSiO₂NP or PSiO₂μP in 250 μL DMF was degassed by sonication for one hour. Then, 6×2 μL of a CDH/NEt₃ (30 mM/60 mM) stock solution were added in one-hour intervals before adding 0.7 mg of pure CDH. The particles were stirred at room temperature under an argon atmosphere overnight and purified by centrifugation and redispersion cycles (3× DMF). Second, the dispersed particles (in 250 μL DMF) were added to a mixture of AuNP (0.4 mg) in toluene (0.5 mL) before placing the vial on an orbital shaker for 18 h. The nanoparticle assemblies were purified by centrifugation (10,000 rpm, 20 min) and redispersion in toluene/DMF (v/v 1:1), DMF and Milli-Q (2×). The silica core was removed as described before.

General procedure for the post-functionalization of PSiO₂NP

If not stated otherwise, the PSiO₂NP were post-functionalized as follows: the particles (50 μL of PSiO₂NP for a typical experiment) were diluted to a total volume of 0.5 mL DMF. To this dispersion, the desired primary amine or thiol bearing compound was added and the mixture was stirred at room temperature for 18 h. The amount of compound used was set to 2.5 mg/50 μL of PSiO₂NP. For cleaving the disulfide bond, we simply added 5–10 mg of TCEP as reducing agent to the particles and stirred the dispersion overnight.

Conflict of Interest

The authors declare no conflict of interest.

[1] P. G. Jeelani, P. Mulay, R. Venkat, C. Ramalingam, *Silicon* **2020**, *12*, 1337.
[2] a) E. D. E. R. Hyde, A. Seyfaee, F. Neville, R. Moreno-Atanasio, *Ind. Eng. Chem. Res.* **2016**, *55*, 8891; b) J.-W. Park, Y. J. Park, C.-H. Jun, *Chem. Commun.* **2011**, *47*, 4860; c) A. Guerrero-Martínez, J. Pérez-Juste, L. M. Liz-Marzán, *Adv. Mater.* **2010**, *22*, 1182.
[3] W. Hou, H. Wang, Y. Cui, Y. Liu, X. Ma, H. Zhao, *Macromolecules* **2019**, *52*, 8404.
[4] H. J. H. Kang, R. F. Ali, M. T. Y. Paul, M. J. Radford, I. Andreu, A. W. H. Lee, B. D. Gates, *Chem. Commun.* **2019**, *55*, 10452.
[5] G. R. Delpiano, M. F. Casula, M. Piludu, R. Corpino, P. C. Ricci, M. Vallet-Regí, E. Sanjust, M. Monduzzi, A. Salis, *ACS Appl. Mater. Interfaces* **2019**, *4*, 11044.
[6] a) A. Wang, Y. Yang, Y. Qi, W. Qi, J. Fei, H. Ma, J. Zhao, W. Cui, J. Li, *ACS Appl. Mater. Interfaces* **2016**, *8*, 8900; b) X. Hao, X. Hu, C. Zhang, S. Chen, Z. Li, X. Yang, H. Liu, G. Jia, D. Liu, K. Ge, X.-J. Liang, J. Zhang, *ACS Nano* **2015**, *9*, 9614; c) Á. A. Beltrán-Osuna, J. E. Perilla, *J. Sol-Gel Sci. Technol.* **2016**, *77*, 480; d) A. Hernández Montoto, A. Llopis-Lorente, M. Gorbe, J. M. Terrés, R. Cao-Milán, B. Díaz de Greñu, M. Alfonso, J. Ibañez, M. D. Marcos, M. Orzáez, R. Villalonga, R. Martínez-Máñez, F. Sancenón, *Chem. Eur. J.* **2019**, *25*, 8471.

Chemistry–A European Journal

Full Paper
doi.org/10.1002/chem.202100547

Chemistry Europe
European Chemical
Societies Publishing

[7] S. Zhou, M. Maeda, E. Tanabe, M. Kubo, M. Shimada, *Langmuir* **2020**, *36*, 2553.

[8] a) Y. Kobayashi, H. Matsudo, T. Li, K. Shibuya, Y. Kubota, T. Oikawa, T. Nakagawa, K. Gonda, *Appl. Nanosci.* **2016**, *6*, 301; b) M. Bouchoucha, R. B. van Heeswijk, Y. Gossuin, F. Kleitz, M.-A. Fortin, *Langmuir* **2017**, *33*, 10531.

[9] X. Li, L. Xing, K. Zheng, P. Wei, L. Du, M. Shen, X. Shi, *ACS Appl. Mater. Interfaces* **2017**, *9*, 5817.

[10] a) Z. S. Qureshi, P. B. Sarawade, I. Hussain, H. Zhu, H. Al-Johani, D. H. Anjum, M. N. Hedhili, N. Maity, V. D'Elia, J.-M. Basset, *ChemCatChem* **2016**, *8*, 1671; b) M. Rocha, C. Fernandes, C. Pereira, S. L. H. Rebelo, M. F. R. Pereira, C. Freire, *RSC Adv.* **2015**, *5*, 5131; c) W. Xie, L. Hu, X. Yang, *Ind. Eng. Chem. Res.* **2015**, *54*, 1505.

[11] a) Y. Shi, H. Zhang, Z. Yue, Z. Zhang, K.-S. Teng, M.-J. Li, C. Yi, M. Yang, *Nanotechnology* **2013**, *24*, 375501; b) A. Bitar, N. M. Ahmad, H. Fessi, A. Elaissari, *Drug Discovery Today* **2012**, *17*, 1147; c) A. C. Patel, S. Li, J.-M. Yuan, Y. Wei, *Nano Lett.* **2006**, *6*, 1042; d) R. R. Castillo, A. Baeza, M. Vallet-Regí, *Biomater. Sci.* **2017**, *5*, 353.

[12] L. Cui, R. Wang, X. Ji, M. Hu, B. Wang, J. Liu, *Mater. Chem. Phys.* **2014**, *148*, 87.

[13] a) S. N. Abdollahi, M. Naderi, G. Amoabediny, *Colloids Surf. A* **2013**, *436*, 1069; b) X. Huang, D. Appelhans, P. Formanek, F. Simon, B. Voit, *Macromolecules* **2011**, *44*, 8351; c) Y. Wang, Y. Yan, J. Cui, L. Hosta-Rigau, J. K. Heath, E. C. Nice, F. Caruso, *Adv. Mater.* **2010**, *22*, 4293; d) G. K. Such, E. Tjipto, A. Postma, A. P. R. Johnston, F. Caruso, *Nano Lett.* **2007**, *7*, 1706.

[14] D. W. Kurka, M. Niehues, B. J. Ravoo, *Langmuir* **2020**, *36*, 3924.

[15] S. Sagebiel, L. Stricker, S. Engel, B. J. Ravoo, *Chem. Commun.* **2017**, *53*, 9296.

[16] P.-E. Rouet, C. Chomette, E. Duguet, S. Ravaine, *Angew. Chem. Int. Ed.* **2018**, *57*, 15757; *Angew. Chem.* **2018**, *130*, 15980.

[17] a) J. G. Croissant, Y. Fatieiev, A. Almalik, N. M. Khashab, *Adv. Healthcare Mater.* **2018**, *7*; b) S. Huh, J. W. Wiench, J.-C. Yoo, M. Pruski, V. S.-Y. Lin, *Chem. Mater.* **2003**, *15*, 4247; c) M. Kalantari, T. Ghosh, Y. Liu, J. Zhang, J. Zou, C. Lei, C. Yu, *ACS Appl. Mater. Interfaces* **2019**, *11*, 13264.

[18] a) J. Zheng, D. Han, S. Zhao, X. Ye, Y. Wang, Y. Wu, D. Dong, J. Liu, X. Wu, L. Zhang, *ACS Appl. Mater. Interfaces* **2018**, *10*, 19922; b) M. Ma, S. Zheng, H. Chen, M. Yao, K. Zhang, X. Jia, J. Mou, H. Xu, R. Wu, J. Shi, *J. Mater. Chem. B* **2014**, *2*, 5828.

[19] A. Noureddine, L. Lichon, M. Maynadier, M. Garcia, M. Gary-Bobo, J. I. Zink, X. Cattoën, M. Wong Chi Man, *Nanoscale* **2015**, *7*, 11444.

[20] P. Espeel, F. E. Du Prez, *Eur. Polym. J.* **2015**, *62*, 247.

[21] a) S. Celasun, D. Remmler, T. Schwaar, M. G. Weller, F. Du Prez, H. G. Börner, *Angew. Chem. Int. Ed.* **2019**, *58*, 1960; *Angew. Chem.* **2019**, *131*, 1984; b) J. O. Holloway, C. Mertens, F. E. Du Prez, N. Badi, *Macromol. Rapid Commun.* **2019**, *40*, e1800685; c) P. Espeel, S. Celasun, P. S. Omurtag, S. Martens, F. E. Du Prez, *Macromol. Rapid Commun.* **2017**, *38*; d) J. O. Holloway, S. Aksakal, F. E. Du Prez, C. R. Becer, *Macromol. Rapid Commun.* **2017**, *38*; e) C. Resetco, D. Frank, N. U. Kaya, N. Badi, F. Du Prez, *ACS Macro Lett.* **2017**, *6*, 277; f) S. Martens, J. van den Begin, A. Madder, F. E. Du Prez, P. Espeel, *J. Am. Chem. Soc.* **2016**, *138*, 14182; g) F. Goethals, S. Martens, P. Espeel, O. van den Berg, F. E. Du Prez, *Macromolecules* **2014**, *47*, 61; h) P. Espeel, L. L. G. Carrette, K. Bury, S. Capenberghs, J. C. Martins, F. E. Du Prez, A. Madder, *Angew. Chem. Int. Ed.* **2013**, *52*, 13261; *Angew. Chem.* **2013**, *125*, 13506; i) P. Espeel, F. Goethals, F. E. Du Prez, *J. Am. Chem. Soc.* **2011**, *133*, 1678.

[22] a) F. Driessen, R. Herckens, P. Espeel, F. E. Du Prez, *Polym. Chem.* **2016**, *7*, 1632; b) F. Driessen, S. Martens, B. de Meyer, F. E. Du Prez, P. Espeel, *Macromol. Rapid Commun.* **2016**, *37*, 947; c) T. Rudolph, P. Espeel, F. E. Du Prez, F. H. Schacher, *Polym. Chem.* **2015**, *6*, 4240; d) Y. Chen, P. Espeel, S. Reinicke, F. E. Du Prez, M. H. Stenzel, *Macromol. Rapid Commun.* **2014**, *35*, 1128; e) P. Espeel, F. Goethals, M. M. Stamenović, L. Petton, F. E. Du Prez, *Polym. Chem.* **2012**, *3*, 1007.

[23] N. U. Kaya, F. E. Du Prez, N. Badi, *Macromol. Chem. Phys.* **2017**, *218*, 1600575.

[24] Z. Su, C. Li, J. Tan, L. Xue, G. Zhang, Y. Yang, Q. Zhang, *J. Colloid Interface Sci.* **2019**, *549*, 201.

[25] a) K. Bruycker, C. Mertens, F. E. Prez, *J. Polym. Sci. Part A* **2019**, *57*, 322; b) S. Reinicke, P. Espeel, M. M. Stamenović, F. E. Du Prez, *Polym. Chem.* **2014**, *5*, 5461.

[26] a) C. Chattaway, S. Belbekhouche, F. E. Du Prez, K. Glinel, S. Demoustier-Champagne, *Langmuir* **2018**, *34*, 5234; b) S. Belbekhouche, S. Reinicke, P. Espeel, F. E. Du Prez, P. Eloy, C. Dupont-Gillain, A. M. Jonas, S. Demoustier-Champagne, K. Glinel, *ACS Appl. Mater. Interfaces* **2014**, *6*, 22457.

[27] C. M. Reese, B. J. Thompson, P. K. Logan, C. M. Stafford, M. Blanton, D. L. Patton, *Polym. Chem.* **2019**, *10*.

[28] J. Zhou, Z. Su, M. Wang, Y. Wang, J. Wang, B. Zhang, Q. Zhang, *Chem. Eng. J.* **2020**, *399*, 125767.

[29] H. Hiramatsu, F. E. Osterloh, *Langmuir* **2003**, *19*, 7003.

[30] a) G. Chen, S. Zhou, G. Gu, L. Wu, *Colloids Surf. A* **2007**, *296*, 29; b) D. Li, X. Sheng, B. Zhao, *J. Am. Chem. Soc.* **2005**, *127*, 6248.

[31] Z. Wang, T. Liu, K. C. Lin, S. Li, J. Yan, M. Olszewski, J. Sobieski, J. Pietrasik, M. R. Bockstaller, K. Matyjaszewski, *J. Inorg. Organomet. Polym.* **2020**, *30*, 174.

[32] H. Wang, M. Peng, J. Zheng, P. Li, *J. Colloid Interface Sci.* **2008**, *326*, 151.

[33] a) L. Stricker, E.-C. Fritz, M. Peterlechner, N. L. Doltsinis, B. J. Ravoo, *J. Am. Chem. Soc.* **2016**, *138*, 4547; b) M. Niehues, P. Tegeder, B. J. Ravoo, *Beilstein J. Org. Chem.* **2019**, *15*, 1407; c) M. Niehues, J. Simke, B. J. Ravoo, *ChemNanoMat* **2020**, *6*, 1743; d) B. P. Nowak, B. J. Ravoo, *Soft Matter* **2020**, *16*, 7299; e) G. Davidson-Rozenfeld, L. Stricker, J. Simke, M. Fadeev, M. Vázquez-González, B. J. Ravoo, I. Willner, *Polym. Chem.* **2019**, *10*, 4106; f) S. Lamping, L. Stricker, B. J. Ravoo, *Polym. Chem.* **2019**, *10*, 683.

[34] A. Bertoluzza, C. Fagnano, P. Finelli, M. A. Morelli, R. Simoni, R. Tosi, *J. Raman Spectrosc.* **1983**, *14*, 386.

[35] a) A. Sánchez-Iglesias, N. Claes, D. M. Solís, J. M. Taboada, S. Bals, L. M. Liz-Marzán, M. Grzelczak, *Angew. Chem. Int. Ed.* **2018**, *57*, 3183; *Angew. Chem.* **2018**, *130*, 3240; b) P.-J. Chen, S.-H. Hu, C.-T. Fan, M.-L. Li, Y.-Y. Chen, S.-Y. Chen, D.-M. Liu, *Chem. Commun.* **2013**, *49*, 892.

[36] a) Z. Nie, A. Petukhova, E. Kumacheva, *Nat. Nanotechnol.* **2010**, *5*, 15; b) Y. Ofir, B. Samanta, V. M. Rotello, *Chem. Soc. Rev.* **2008**, *37*, 1814; c) F. Wang, S. Cheng, Z. Bao, J. Wang, *Angew. Chem. Int. Ed.* **2013**, *52*, 10348; *Angew. Chem.* **2013**, *125*, 10534; d) P. B. Landon, A. H. Mo, C. Zhang, C. D. Emerson, A. D. Printz, A. F. Gomez, C. J. DeLaTorre, D. A. M. Colburn, P. Anzenberg, M. Eliceiri, C. O'Connell, R. Lal, *ACS Appl. Mater. Interfaces* **2014**, *6*, 9937; e) A. Le Beulze, S. Gomez-Graña, H. Gehan, S. Mornet, S. Ravaine, M. Correa-Duarte, L. Guerrini, R. A. Alvarez-Puebla, E. Duguet, E. Pertreux, A. Crut, P. Maioli, F. Vallée, N. Del Fatti, O. Erseng, M. Treguer-Delapierre, *Nanoscale* **2017**, *9*, 5725.

[37] a) C. Hanske, M. N. Sanz-Ortiz, L. M. Liz-Marzán, *Adv. Mater.* **2018**, e1707003; b) A. F. Moreira, C. F. Rodrigues, C. A. Reis, E. C. Costa, I. J. Correia, *Microporous Mesoporous Mater.* **2018**, *270*, 168.

[38] a) D. E. Discher, A. Eisenberg, *Science* **2002**, *297*, 967; b) A. P. Johnston, G. K. Such, S. L. Ng, F. Caruso, *Curr. Opin. Colloid Interface Sci.* **2011**, *16*, 171; c) W. C. de Vries, D. Grill, M. Tesch, A. Ricker, H. Nüsse, J. Klingauf, A. Studer, V. Gerke, B. J. Ravoo, *Angew. Chem. Int. Ed.* **2017**, *56*, 9603; *Angew. Chem.* **2017**, *129*, 9736; d) W. C. de Vries, S. Kudruk, D. Grill, M. Niehues, A. L. L. Matos, M. Wissing, A. Studer, V. Gerke, B. J. Ravoo, *Adv. Sci.* **2019**, *6*, 1901935; e) F. Cuomo, A. Ceglie, A. de Leonardis, F. Lopez, *Catalysts* **2019**, *9*, 1; f) V. Sharma, A. Sundaramurthy, *ACS Appl. Mater. Interfaces* **2019**, *4*, 628.

[39] a) M. N. Antipina, G. B. Sukhorukov, *Adv. Drug Delivery Rev.* **2011**, *63*, 716; b) L. J. de Cock, S. de Koker, B. G. de Geest, J. Grooten, C. Vervaet, J. P. Remon, G. B. Sukhorukov, M. N. Antipina, *Angew. Chem. Int. Ed.* **2010**, *49*, 6954; *Angew. Chem.* **2010**, *122*, 7127; c) S. de Koker, R. Hoogenboom, B. G. de geest, *Chem. Soc. Rev.* **2012**, *41*, 2867.

[40] a) J. P. Leung, S. Wu, K. C. Chou, R. Signorell, *Nanomaterials* **2013**, *3*, 86; b) J. Z. Zhang, *J. Phys. Chem. Lett.* **2010**, *1*, 686.

[41] W. C. de Vries, M. Niehues, M. Wissing, T. Würthwein, F. Mäsing, C. Fallnich, A. Studer, B. J. Ravoo, *Nanoscale* **2019**, *11*, 9384.